

Geophysical Research Letters®



RESEARCH LETTER

10.1029/2023GL103076

Key Points:

- Aerosol-induced absorptive-heating increases stratospheric water vapor (SWV) by up to 17% at 18 months post-eruption in a Pinatubo-like experiment
- Analyzing simulations by El Niño–Southern Oscillation (ENSO) variability show an 80% larger peak SWV increase occurs if an eruption is followed by a La Niña phase
- The timing of peak SWV increase occurs when volcanic-aerosol-induced heating reaches the tropopause, with ENSO modulation of tropical upwelling

Supporting Information:

Supporting Information may be found in the online version of this article.

Correspondence to:

X. Zhou,
x.zhou1@leeds.ac.uk

Citation:

Zhou, X., Mann, G. W., Feng, W., Dhomse, S. S., & Chipperfield, M. P. (2023). The influence of internal climate variability on stratospheric water vapor increases after large-magnitude explosive tropical volcanic eruptions. *Geophysical Research Letters*, 50, e2023GL103076. <https://doi.org/10.1029/2023GL103076>






Received 8 APR 2023

Accepted 2 SEP 2023

Author Contributions:

Conceptualization: Xin Zhou
Data curation: Xin Zhou
Formal analysis: Xin Zhou
Funding acquisition: Xin Zhou
Investigation: Xin Zhou
Methodology: Xin Zhou
Project Administration: Xin Zhou
Resources: Graham W. Mann, Wuhu Feng, Sandip S. Dhomse, Martyn P. Chipperfield
Software: Xin Zhou

The Influence of Internal Climate Variability on Stratospheric Water Vapor Increases After Large-Magnitude Explosive Tropical Volcanic Eruptions

Xin Zhou^{1,2} , Graham W. Mann^{2,3} , Wuhu Feng^{2,3} , Sandip S. Dhomse^{2,4} , and Martyn P. Chipperfield^{2,4} 

¹Plateau Atmosphere and Environment Key Laboratory of Sichuan Province, School of Atmospheric Sciences, Chengdu University of Information Technology, Chengdu, China, ²School of Earth and Environment, University of Leeds, Leeds, UK, ³National Centre for Atmospheric Science, University of Leeds, Leeds, UK, ⁴National Centre for Earth Observation, University of Leeds, Leeds, UK

Abstract Substantial and prolonged enhancements in stratospheric water vapor (SWV) have occurred after large-magnitude explosive tropical volcanic eruptions, with modified tropopause entry caused by aerosol-absorptive heating. Here, we analyze the timing and longevity of heating-driven post-eruption SWV changes within CMIP6-VolMIP short-term climate-response experiments with the UK Earth System Model (UKESM1). We find aerosol-absorptive heating causes peak SWV increases of 17% (~1 ppmv) and 10% (0.5 ppmv) at 100 and 50 hPa, at ~18 and ~23 months after a Pinatubo-like eruption, respectively. We track the temperature response in the tropical lower stratosphere and identify the main SWV increase occurs only after the descending aerosol heating reaches the tropopause, suggesting a key role for aerosol microphysical processes (sedimentation rate). We explore how El Niño–Southern Oscillation variability modulates this effect. Post-eruption SWV increases are ~80% stronger for the La Niña phase compared to the ensemble mean. Tropical upwelling strongly mediates this effect.

Plain Language Summary Strong volcanic eruptions, such as the 1991 eruption of Mt Pinatubo, inject a large amount of SO₂ directly into the stratosphere, thereby enhancing the stratospheric aerosol layer and causing a short-term climatic perturbation. Another substantial part of the climatic influence is the change in stratospheric water vapor (SWV), which affects the chemical processes and the radiative budget of the atmosphere. Along with near-instantaneous injection of water vapor into the stratosphere, volcanic eruptions can indirectly enhance the entry of water vapor into the stratosphere through aerosol-induced tropopause heating. This work analyses Earth system model experiments designed to explore how volcanic impacts combine with internal climate variability. We find that peak SWV entry mixing ratios occur only within the second post-eruption year, consistent with the substantially lagged timing of SWV increase seen in post-Pinatubo satellite measurements. This analysis provides a new perspective on the temporal evolution of the observed post-Pinatubo SWV increase and an improved quantification of its impacts.

1. Introduction

The volcanic forcing of climate arises primarily from emitted sulfur dioxide (SO₂), forming a sulfate aerosol haze, that scatters solar radiation back to space, and absorbs a relatively lower amount of terrestrial long-wave radiation (e.g., Lacis et al., 1992). After major tropical eruptions, a localized heating from this volcanic aerosol absorption increases stratospheric water vapor (SWV) via greater tropopause entry (e.g., Joshi & Shine, 2003). Some volcanic eruptions can emit large amounts of water vapor directly into the stratosphere, for example, after 1883 Krakatau (Joshi & Jones, 2009; Self, 1992; Self & Sparks, 1978) and from the January 2022 Hunga-Tonga eruption (Millán et al., 2022).

Attributing volcanic SWV changes due to volcanically enhanced aerosol is complex because there are few sufficiently large eruptions in the observational era. There is also substantial internal SWV variability associated with the El Niño–Southern Oscillation (ENSO) and Quasi-Biennial Oscillation (QBO) (see Garfinkel et al., 2013; Rosenlof & Reid, 2008; Scaife et al., 2003). There has also been a gradual SWV increase from decadal changes in the strength of the stratospheric circulation (e.g., Dhomse et al., 2008; Randel et al., 2006; Rosenlof et al., 2001) and from increased methane oxidation (e.g., Considine et al., 2001; Evans et al., 1998). An alternative approach is

© 2023. The Authors.

This is an open access article under the terms of the [Creative Commons Attribution License](https://creativecommons.org/licenses/by/4.0/), which permits use, distribution and reproduction in any medium, provided the original work is properly cited.

Supervision: Xin Zhou
Validation: Xin Zhou
Visualization: Xin Zhou
Writing – original draft: Xin Zhou
Writing – review & editing: Xin Zhou, Graham W. Mann, Wuhu Feng, Sandip S. Dhomse, Martyn P. Chipperfield

to isolate the volcanic signal with the aid of model (e.g., Kilian et al., 2020; Kroll et al., 2021; Löffler et al., 2016), but large uncertainties still exist due to different models, forcing input and internal climate variability (Zanchettin et al., 2016).

We analyze the UKESM VolMIP volc-pinatubo-full experiment (see Zanchettin et al., 2016), specifically designed to enable to separation of the volcanic signal from internal climate variability within atmosphere-ocean coupled Earth System Model simulations. Section 2 and 3 detail our experimental design, methods, and the key characteristics of the model performance related to the SWV entry mechanism. Section 4 presents our key results about modification of SWV entry mixing ratios followed by Summary and discussion in Section 5.

2. Models

The model experiments apply version 1 of the UK Earth System Model (UKESM1, Sellar et al., 2019), built around the Global Atmosphere 7.1 (GA7.1) configuration of the UK Met Office Unified Model (Mulcahy et al., 2018; Walters et al., 2019) with coupling to the NEMO ocean model (Storkey et al., 2018), and the JULES land-surface model (Best et al., 2011). The atmosphere model has a well-resolved stratosphere achieving an internally generated QBO with stratosphere-troposphere chemistry (Archibald et al., 2020) and tropospheric aerosol radiative forcing from the GLOMAP-mode modal aerosol microphysics model (Bellouin et al., 2013; Dhomse et al., 2014; Mann et al., 2010). Briefly, the experiment design is a 27-member “initial conditions ensemble” of 36-month “Pinatubo-aerosol forcing only” simulations, each branched off from the parent Pre-Industrial (PI-ctrl) control runs (see Table S1 in Supporting Information S1). These simulations are designed to explore the sensitivity of volcanic impacts to internal climate variations by selecting years from the PI-ctrl to sample modes of tropical and Atlantic variability in the winter after the June 15th eruption. The 27 ensemble simulations include 3 simulations for each of warm, neutral, and cold ENSO phases, and positive, neutral, and negative North Atlantic Oscillation (NAO) indices. All 27 initialization files for the UKESM PI-ctrl were selected so that the mean QBO phase was in easterly phase after eruption from July 1991 to December 1991 (based on a 50 hPa mean tropical zonal wind diagnostic).

3. Methods

Here we analyze the UKESM-simulated SWV response from this VolMIP “volc-pinatubo-full” experiment (Zanchettin et al., 2016), analyzing co-variations with temperature, heating rates and tropical upwelling. All anomalies in the Pinatubo-forced runs are calculated with respect to the PI control runs. A two-tailed *student-t* test is performed to detect the significance of the anomalies. The modulation of volcanic impacts by ENSO and NAO variability is investigated by comparing the subsampled volcanic-forced runs and PI-ctrl runs under the same states of ENSO or NAO. The Clausius–Clapeyron equation is used to assess the co-variation of temperature and water vapor to demonstrate the saturated air in the tropical tropopause region, for the “freeze drying” effect hypothesized to generate the observed post-eruption SWV moist anomaly.

The transformed Eulerian mean (TEM) residual velocity is used as a metric for quantifying the overall strength of the Brewer–Dobson circulation (BDC) (e.g., Butchart & Scaife, 2001; Seviour et al., 2012). The vertical ($\bar{\omega}^*$) component of the TEM residual circulation, which we refer to simply as “tropical upwelling”, is calculated via Equation 3.5.1 in Andrews et al. (1987):

$$\bar{\omega}^* = \bar{\omega} + (\cos\phi)^{-1} \left[\cos\phi \left(\overline{v'\theta' / \theta_p} \right) \right]_{\phi} \quad (1)$$

with θ the potential temperature, $\bar{\omega}$ the zonal-mean vertical velocity in pressure coordinates, and subscripts p and ϕ denoting derivatives with respect to pressure and latitude.

4. Results

4.1. Timing and Longevity of the SWV Increase

Figure 1 shows the UKESM-predicted SWV anomalies caused by the Pinatubo aerosol on the 27-member ensemble mean. Peak SWV enhancement at 100 hPa occurs 17 months after the eruption, with a magnitude of ~ 1.0 ppmv on the ensemble mean. The SWV enhancement first becomes significant around 3 months post-eruption,

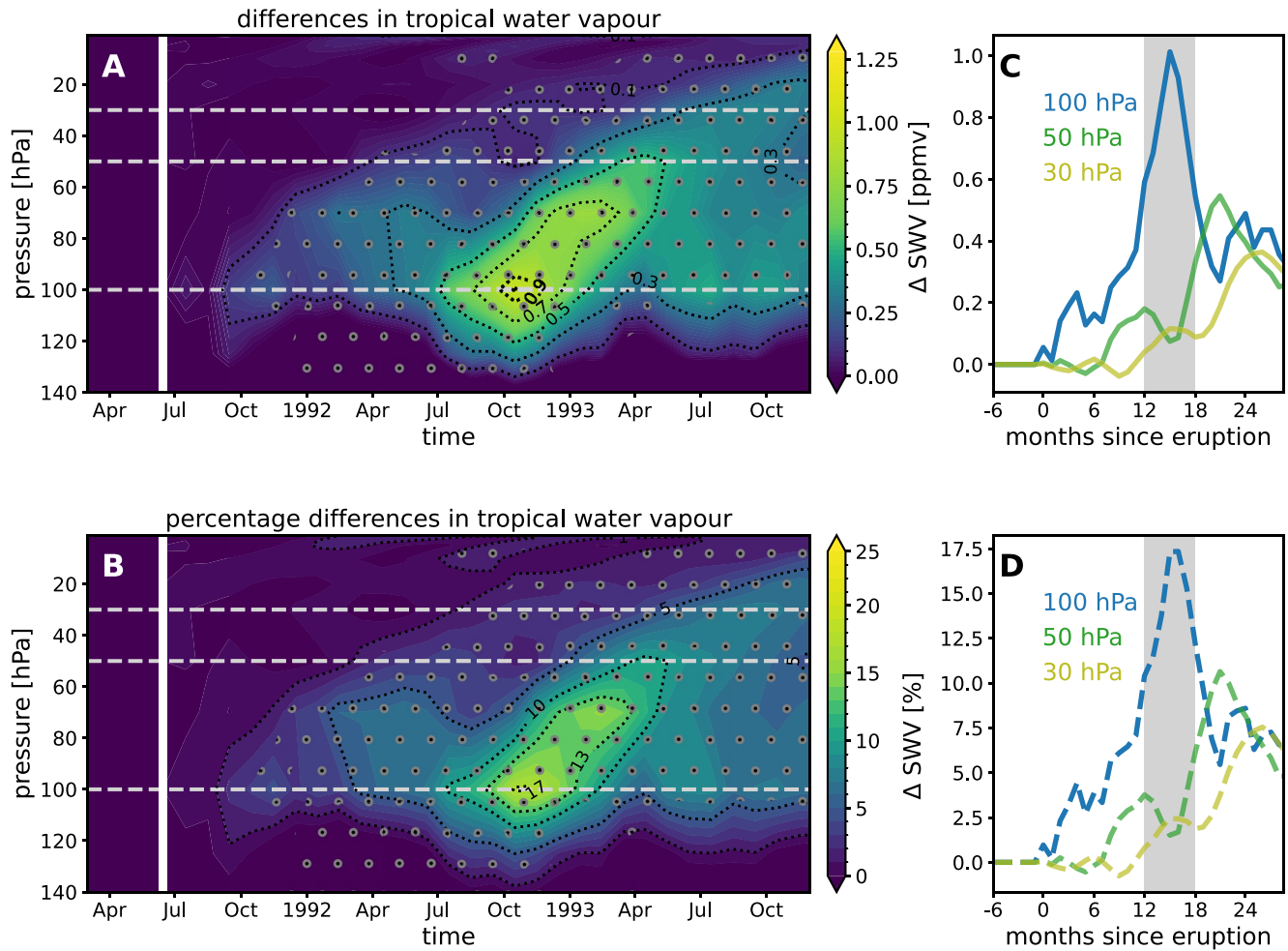


Figure 1. SWV response to Pinatubo-like volcanic aerosol forcing. (a) Absolute and (b) percentage difference in water vapor above 140 hPa in the tropics (23°S–23°N) averaged between volcanically perturbed and unperturbed ensemble runs, and (c, d) their time series at 100 hPa, 50 hPa, and 30 hPa. Regions covered by dots indicate statistically significant differences with confidence of 95% (based on Student's *t*-test).

but remains below 10% (Figures 1b and 1d) for the entire first year after the eruption. Months 12–18 after the eruption see a sudden change to a rapid moistening, with the enhancement transported upwards within the tropical stratospheric reservoir. A slight reduction in the enhancement is seen into DJF 1991, which likely reflects the 6-month-period variation associated with the BDC seasonal cycle that we will discuss later. It is worth noting that the VolMIP experiment design produces a pre-industrial-BDC-strength upwelling, which is slower than will have been the case after Pinatubo (e.g., Eichinger et al., 2019).

The observed signal of post-eruption water vapor increase in the tropical stratosphere can be seen here to correspond to an initial phase of slow but steady increase into a second phase of much steeper increase in the second post-eruption year. Here this reaches a maximum in October 1992; the increase from 10% to 17% above background level occurring in just 4 months. Other post-volcanic changes of radiatively active species such as methane (Dlugokencky et al., 1994, 1996) and ozone (Hofmann & Solomon, 1989; Kinne et al., 1992) will also occur, alongside the localized aerosol heating, and the co-variations explored in this isolated volcanic-forcing experiment enable the balance among these drivers to be assessed.

This amplification of SWV entry in the winter half of the second post-eruption year differs from previous studies using general circulation models (GCMs) (Joshi & Shine, 2003, their Figure 3b) or simpler 2D models (Considine et al., 2001, their Figure 16b) which found that peak SWV entry at 100 hPa occurs in the first eruption year. Using nudged interactive chemistry-climate model simulations, Löffler et al. (2016) showed a triple peak in SWV entry at similar levels, each peak an increase of more than 40%. A follow-up study by Kilian et al. (2020) attributes this

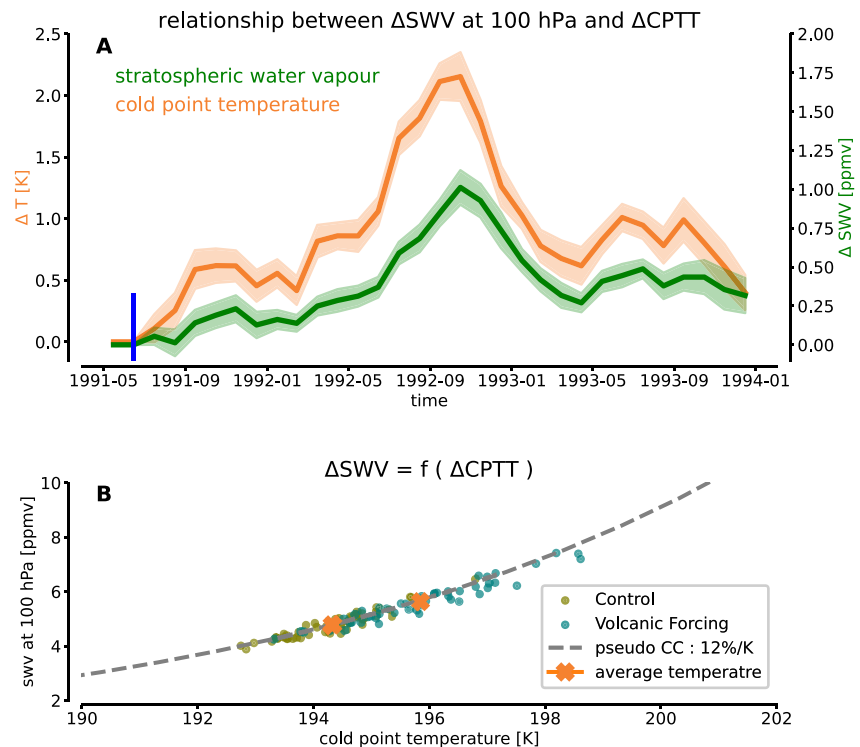


Figure 2. SWV entry constrained by cold-point temperature. Differences in the inner tropical (5°S – 5°N) (a) cold point temperature (K) and stratospheric water vapor (ppmv) between volcanically perturbed and unperturbed ensemble runs. The ensemble means are shown with their standard errors. The time of the volcanic eruption is indicated by a vertical blue line. (b) The seasonal averages of specific humidity (ppmv) at the cold point as function of cold-point temperature for the peak season (October–November–December 1992). Values for each individual ensemble member are shown as dots for the inner tropics. An approximation (see text) for the Clausius–Clapeyron equation at this temperature range with a 12% increase of specific humidity per K is indicated by a dashed gray line. The ensemble mean cold-point temperatures and specific humidity for volcanically perturbed and unperturbed ensemble runs are indicated in orange.

increase to the volcanic aerosol heating effect, separating the heating-driven changes from the volcanic aerosol chemistry effect, which by contrast leads to dehydration in the lower stratosphere after a cooling due to ozone loss. Kroll et al. (2021) showed an increase of 25% at corresponding levels with two peaks in the same year 1992, but used a GCM without interactive chemistry. HALOE satellite measurements appear to be contaminated by volcanic aerosol in the first post-eruption year, but it did see an increase in SWV entry of around 1 ppmv in the tropics (12°S – 12°N) in late 1992 (Mote et al., 1996, their plate 1a; Fueglistaler, 2012). Our results are in good agreement with the observational records for the increase in the SWV entry in the second eruption year when the observations are more reliable. Another notable feature in Figure 1 is a smaller peak SWV increase of 17% in our simulations, which is lower than the range from 25% to 45% at the corresponding level in earlier modeling studies mentioned above.

The timing of SWV increase mirrors in the tropical tropopause temperature due to the cold-point temperature “freeze-drying” mechanism (Figure 2). Although the cold point is defined as the lowest temperature in the inner tropical (5°S – 5°N) tropopause layer region, a pressure level of 100 hPa is used as an approximation for the tropical cold-point tropopause level. The anomalous warming of cold-point temperature rises to a maximum of (2.24 ± 0.23) K and peaks in October 1992, leading to the peak for the inner tropical water vapor anomalies of (1.07 ± 0.12) ppmv (Figure 2a). The vertical temperature profiles are included in the Supplement (Figure S1 in Supporting Information S1) with pronounced separation of cold-point temperature response during the peak entry season October–November–December 1992, indicating a significant increase of cold-point temperature in the second post-eruption year among different ensemble members. The water vapor entry value and tropical cold-point tropopause temperature relationship in the peak SWV entry season in October–November–December 1992 fits the line which approximates the Clausius–Clapeyron equation very well under this temperature range assuming the atmosphere around the cold point is saturated in the unper-

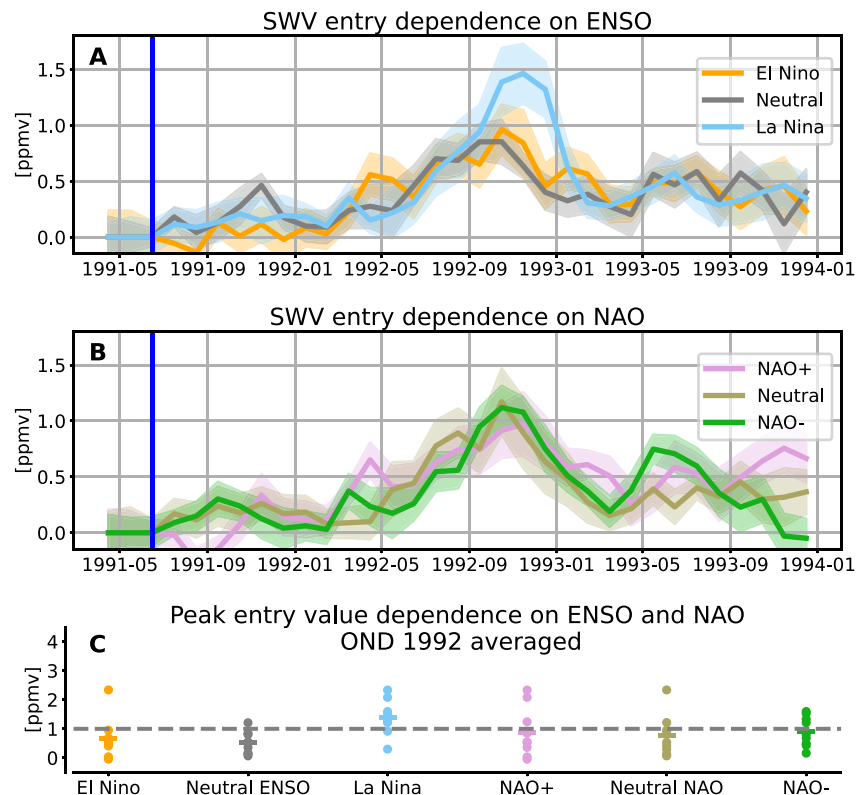


Figure 3. Heating-driven volcanic entry dependence on ENSO and NAO. (a, b) Stratospheric water vapor anomalies (ppmv) averaged over the subsampled ensemble members with different ENSO and NAO conditions. (c) Averaged SWV anomalies in the inner tropical region in October–November–December 1992 as a function of different ENSO and NAO conditions for all ensemble members. Each point represents one ensemble member; the horizontal lines denote the subsampled ensemble mean under the respective conditions.

turbed runs (Figure 2b). The ensemble mean of the simulated entry value agrees well with the seasonal-mean value predicted using the equation, with only a very small discrepancy (less than 1% of the predicted value by the Clausius–Clapeyron equation).

We now assess the sensitivity of the timing and longevity of this heating-driven volcanic entry to the internal variabilities involving ENSO and NAO by comparing the SWV anomalies under different ENSO and NAO phases (Figure 3). The QBO phase is the same for each member (Figure S2 in Supporting Information S1) so that we can ensure that the differences of the SWV entry between each member are attributed to the different background state associated with ENSO and NAO. In general, the temporal evolution of additional SWV entry shows consistent features in the mean of 27 ensemble members, indicating the robustness of our results. The dependence of the SWV entry value on NAO is relatively small, but it is substantially larger in 9 members under the cold ENSO phase (La Niña) compared with the neutral ENSO and warm ENSO (El Niño) phases. The entry value averaged in the peak months (October–November–December 1992) is 1.39 ppmv for the subsampled ensemble (9 members) means under the La Niña phase; this exceeds all the other ensemble (18 members) means (0.58 ppmv) by ~80%. In addition, this peak increase is more persistent in case of La Niña than other phases of ENSO. While ENSO's net effect on the zonal mean SWV entry is still not clear (see review by Domeisen et al., 2019), our result supports evidence from earlier observations and model studies by Garfinkel et al. (2018, 2021) that La Niña acts to moisten the stratosphere in Northern Hemisphere winter relative to neutral ENSO. The dynamical mechanism for this La Niña enhancement is discussed in detail later. However, El Niño shows a rather weak, if any, moistening effect in the ensemble mean, although one member is distinct from the ensemble mean showing a strong enhancement in the SWV entry. The warming of tropical cold-point tropopause coherently exhibits strong dependence under different ENSO phases, with the largest temperature increase in case of La Niña exceeding those under El Niño and neutral ENSO phases (Figure S3 in Supporting Information S1). A note of caution is due here since the ensemble size is reduced by the sub-sampling analysis.

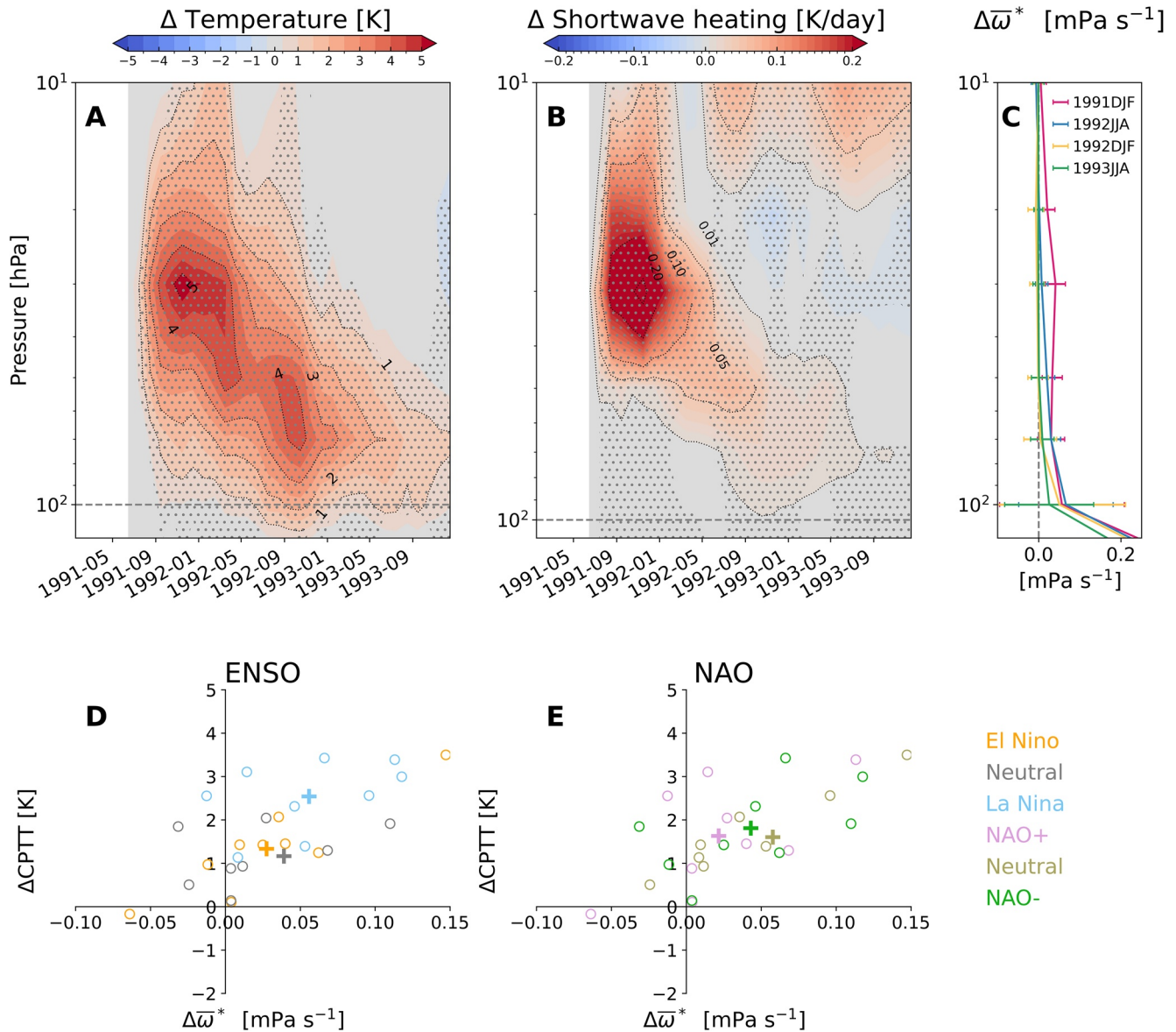


Figure 4. Descending warming signal driven by a decelerated tropical upwelling. (a, b) Differences in the temperature and shortwave heating rate averaged in the inner tropics. (c) Seasonal mean of the differences in $\bar{\omega}^*$ profiles, with means taken within the latitude near 15° in summer hemisphere. The solid line represents the ensemble mean; the error bars represent the ensemble standard deviations. (d, e) Differences in the tropical cold-point tropopause temperature (CPTT) as a function of differences in $\bar{\omega}^*$ at 100 hPa averaged in peak entry season (October–November–December 1992). Each circle represents one ensemble member; the plus signs denote the subsampled ensemble mean under the respective conditions.

4.2. Causes of the Timing and Longevity of Heating-Driven Volcanic Entry

We now investigate in detail the thermodynamics leading to the prolonged volcanic entry. The plot of tropical temperature anomalies shows a clear signal of the descending anomalous heating over time, with the largest signal descending to the cold-point tropopause (100 hPa) during the period of October–November 1992 (Figure 4a), in agreement with the peak months for volcanic entry. Consistent with this, the anomalous shortwave heating maximum is first detected in the region of highest aerosol concentrations near 30 hPa and descends to the tropopause layer at the same point of two years after eruption (Figure 4b). The longwave heating, with a relatively smaller rate, also contributes to anomalous heating (Figure S4 in Supporting Information S1). The positive shortwave heating anomalies in the upper stratosphere one year after eruption are

probably associated with increased ozone concentrations above aerosol layer (Richter et al., 2017). We see a clear stratospheric warming related to shortwave heating due to volcanic aerosol and this correlation is in line with other modeling and observational studies (e.g., Ming & Hitchcock, 2022; Robock, 2000; Stenchikov et al., 1998). The joint descending signal in temperature and shortwave heating anomalies also hints that there is an anomalous downward vertical motion in the tropical stratosphere. Gravitational settling of the Pinatubo aerosol can descend the radiative heating after eruption (Dhomse et al., 2014), but a prolonged downward motion persisting for two years is very possibly linked with the changes in the stratospheric circulation. We diagnose the tropical branch of the BDC as a proxy for the Lagrangian-mean motion in the stratosphere. Figure 4c shows changes in the vertical profile of seasonal averaged tropical upwelling after eruption. A generally decelerated tropical upwelling in the lower stratosphere in response to volcanic forcing is found, explaining the persistent downward motion in temperature and shortwave heating anomalies. There are significant differences at latitudes near 15° in both hemispheres between the ensemble means of Pinatubo-aerosol-forced and control simulations. Map views of the tropical upwelling at 100 hPa in response to volcanic forcing and a meridional view of the seasonal averaged vertical structure of the BDC for control and perturbed runs, as well as their difference in 1992 winter, are included in the Supplement (Figures S5 and S6 in Supporting Information S1). Both the shallow and deep branches show a clear deceleration with the upwelling shifting into the summer hemisphere. The largest differences do not occur at the equator because of the seasonal shift of tropical upwelling toward the summer hemisphere (Randel et al., 2008). We show in Figure 4d and Figure S6 in Supporting Information S1 the vertical structure of $\bar{\omega}^*$ with significantly slowed upwelling throughout the lower stratosphere, thus the results are not sensitive to the level chosen in the lower stratosphere.

This result is very different from many previous findings using models in which an intensified BDC was shown (e.g., Abalos et al., 2015; Aquila et al., 2013; DallaSanta et al., 2021; Kinne et al., 1992; Pitari, 1993; Pitari & Mancini, 2002; Toohey et al., 2014). However, Garfinkel et al. (2017) and Garcia et al. (2011) found the post-volcanic BDC response was an acceleration effect, but mainly in the mid and upper stratosphere, and Garfinkel et al. (2017) showed very little change in the BDC in the lower stratosphere (see their Figure 6b). Diallo et al. (2012, 2017), using Lagrangian model (cLaMS) and ERA-Interim reanalysis data, and Muthers et al. (2016), using climate model (SOCOL), suggested an increase of age-of-air after Pinatubo, corresponding to a slower BDC. DallaSanta et al. (2019) using a simplified model showed a poleward shifting and strengthening jet in response to the enhanced meridional gradient of temperature by tropical stratospheric warming, which is also found in our more detailed model (Figure S7 in Supporting Information S1). This anomalous wind pattern alters the propagation of wave activities. The slowdown in tropical upwelling occurs as a result of a decrease in wave forcing in the subtropics diagnosed by the anomalous EP flux divergence (Figure S7 in Supporting Information S1). Meanwhile, the vertical stability of the atmosphere is enhanced in the tropical lower stratosphere (Figure S8 in Supporting Information S1), which also acts to reduce tropical upwelling (DallaSanta et al., 2021). Together these results indicate an overall deceleration of the tropical upwelling in response to the volcanic eruption. The 3-month lag corresponds to the time for the convergence of extratropical stratosphere to the equilibrium as shown in the zonal wind response, which also explains the time lag we see in the SWV entry (Figure 1). This signal in the tropical tropospheric circulation persists and maintains a significant value lasting throughout two years after eruption, especially in the winter seasons. The aerosol sedimentation in the first few months and the persistent changes in tropical upwelling response, together, serve as a critical mechanism for bringing down the volcanic aerosol and thus shortwave heating to the tropical tropopause.

The role of internal variabilities involving ENSO and NAO in modulating the volcanic entry value is analyzed by comparing the response of tropical upwelling in subsampled simulations according to their different background states. Figures 4d and 4e show the response of cold-point tropopause temperature as a function of tropical upwelling at 100 hPa for these members averaged in the peak entry season (October–November–December 1992). Different colors are used to distinguish different ENSO and NAO phases. These members follow the relationship that an anomalously decelerated tropical upwelling leads to adiabatic warming of the tropical cold-point tropopause, as proved by previous studies (e.g., Holton et al., 1995; Thompson & Solomon, 2005). Almost all members for La Niña, except one, simulate a decelerated tropical upwelling and thereby a warming in the tropical cold-point tropopause temperature. These 9 members for La Niña are in general well separated from the other 18 members for neutral ENSO and El Niño, showing more decelerated tropical upwelling and more warmed cold-point tropopause temperature. This explains the large SWV entry value in peak season

in case of La Niña, exceeding both El Niño and neutral ENSO ensemble mean shown in Figures 3a and 3c. In addition, the slowdown in the tropical upwelling is more persistent than the other two ENSO phases until decaying after December 1992 (Figure S9 in Supporting Information S1). The comprehensive dynamics for the slowdown in tropical upwelling in the lower tropical stratosphere during La Niña and acceleration in El Niño via modulating the propagation and dissipation of the gravity waves are discussed in Calvo et al. (2010). However, one member for El Niño is well beyond the other members, showing strong decelerated tropical upwelling and warmed tropical tropopause temperature (Figure 4d) and corresponding to the member with the highest SWV entry value among the 9 El Niño members in the peak season (Figure 3c). The reason for this one-member discrepancy is not clear, which is possibly linked with the nonlinearity in the SWV response to El Niño strength. The members for different NAO phases have a large spread and their ensemble means are very close (Figure 4e), leading to the small differences in their ensemble means for the SWV entry value in peak season (Figure 3c).

5. Summary and Discussion

Analysis of UKESM1 model simulations suggests that dynamical response of the SWV from the volc-pinatubo-full experiment reveals a two-phase increase in SWV with a slow increase in the first year, followed by a second phase of much steeper increase for months 12–18 after eruption. The peak SWV enhancement at 100 hPa is seen 17 months after eruption, with a magnitude of ~ 1.0 ppmv ($\sim 17\%$ increase over background levels) on the ensemble mean. This significant moistening effect lasts for more than 2 years, indicating its importance in understanding the SWV interannual variability and long-term change. This response, both the increased level and the time evolution, is captured by the changes in the tropical cold-point temperature. By comparing simulations with very different background dynamical conditions including positive, neutral and negative ENSO and NAO phases, we determine statistically robust volcanic signals from background dynamical variability. We show that La Niña leads to a more persistent SWV entry after eruption, with its peak value exceeding $\sim 80\%$ of the other two ENSO phases. The peak SWV entry in the second eruption year occurs when the volcanic-aerosol-induced heating reaches the tropopause, with ENSO phase at 6–9 months post-eruption strongly modulating the dynamically induced SWV increase.

A caveat is that our result on tropical SWV entry is driven by the tropical tropopause temperature response to the volcanic eruption, an effect that may be dependent on the prescribed volcanic aerosol forcing data set (Rieger et al., 2020), forcing implementation and radiation scheme used in climate models (Zanchettin et al., 2022a), and more generally how the model describes the volcanic plume (Stenchikov et al., 2021). Whilst the 27 ensemble members and VolMIP experiment design have enabled to quantify ENSO modulation of heating-driven SWV increases within an easterly post-eruption QBO regime, a future protocol with a larger ensemble would potentially enable to explore the effect within westerly or transitory QBO phase. Improving our current knowledge of volcanic injection is a necessary step to understand its climate perturbation. Future experiments with both direct injection and modified tropopause entry, and work to fully consider the internal variabilities including ENSO, and NAO, are needed.

Data Availability Statement

The time series used in the analysis are available from the World Data Center for Climate (WDCC) public repository at the Deutsches Klimarechenzentrum (DKRZ) (https://cera-www.dkrz.de/WDCC/ui/Compact.jsp?acronym=VolMIP_pC, https://cera-www.dkrz.de/WDCC/ui/Compact.jsp?acronym=VolMIP_volc_UKESM1; Zanchettin et al., 2022b, 2022c). Figures were made with python open-source software libraries: aostools (Jucker, 2022), matplotlib (Hunter, 2007), numpy (Harris et al., 2020), scipy (Virtanen et al., 2020), and xarray (Hoyer et al., 2022). Code to produce the figures in this manuscript is available from <https://doi.org/10.5281/zenodo.7810072> (Zhou, 2023).

References

- Abalos, M., Legras, B., Ploeger, F., & Randel, W. J. (2015). Evaluating the advective Brewer-Dobson circulation in three reanalyses for the period 1979–2012. *Journal of Geophysical Research*, *120*(15), 7534–7554. <https://doi.org/10.1002/2015JD023182>
- Andrews, D. G., Holton, J. R., & Leovy, C. B. (1987). *Middle atmosphere dynamics*. Academic press.

Acknowledgments

X. Zhou acknowledges funding from the National Natural Science Foundation of China (42275059; 42175042), China Scholarship Council (201908510032), Natural Science Foundation of Sichuan Province (2023NSFSC0246; 2022NSFSC1056), and Chengdu University of Information Technology (KYTZ202218). M.P. Chipperfield acknowledges funding from the NCEO TerraFirma project and NERC LSO3 project NE/V011863/1. S.S. Dhomse received funding from the UK National Centre for Atmospheric Science (NCAS), via the 1-year funded-extension to the ACSIS long-term science programme on the North Atlantic climate system (NE/N018001/1). G.W. Mann received funding from NERC standard grant project MeteorStrat (NE/N011222/1) and from NCAS during the main phase of the ACSIS project. W. Feng also acknowledges funding from the NCAS single-centre Long-term Science programme (NE/R015244/1), within the “Climate and High Impact Weather” theme. The UKESM simulations were carried out on the joint UK Met Office and Natural Environment Research Council (NERC) MONSooN supercomputing system (“Met Office and NERC Supercomputer Nodes”), with data analysis using the UK collaborative “Joint Analysis System Meeting Infrastructure Needs” super-data-cluster facility (JASMIN).

- Aquila, V., Oman, L. D., Stolarski, R., Douglass, A. R., & Newman, P. A. (2013). The response of ozone and nitrogen dioxide to the eruption of Mt. Pinatubo at southern and northern midlatitudes. *Journal of the Atmospheric Sciences*, 70(3), 894–900. <https://doi.org/10.1175/JAS-D-12-0143.1>
- Archibald, A. T., O'Connor, F. M., Abraham, N. L., Archer-Nicholls, S., Chipperfield, M. P., Dalvi, M., et al. (2020). Description and evaluation of the UKCA stratosphere–troposphere chemistry scheme (StratTrop v1.0) implemented in UKESM1. *Geoscientific Model Development*, 13(3), 1223–1266. <https://doi.org/10.5194/gmd-13-1223-2020>
- Bellouin, N., Mann, G. W., Woodhouse, M. T., Johnson, C., Carslaw, K. S., & Dalvi, M. (2013). Impact of the modal aerosol scheme GLOMAP-mode on aerosol forcing in the Hadley centre global environmental model. *Atmospheric Chemistry and Physics*, 13(6), 3027–3044. <https://doi.org/10.5194/acp-13-3027-2013>
- Best, M. J., Pryor, M., Clark, D. B., Rooney, G. G., Essery, R. L. H., Ménard, C. B., et al. (2011). The joint UK land environment simulator (JULES), model description – Part 1: Energy and water fluxes. *Geoscientific Model Development*, 4(3), 677–699. <https://doi.org/10.5194/gmd-4-677-2011>
- Butchart, N., & Scaife, A. A. (2001). Removal of chlorofluorocarbons by increased mass exchange between the stratosphere and troposphere in a changing climate. *Nature*, 410(6830), 799–802. <https://doi.org/10.1038/35071047>
- Calvo, N., Garcia, R. R., Randel, W. J., & Marsh, D. R. (2010). Dynamical mechanism for the Increase in tropical upwelling in the lowermost tropical stratosphere during warm ENSO events. *Journal of the Atmospheric Sciences*, 67(7), 2331–2340. <https://doi.org/10.1175/2010JAS3433.1>
- Conside, D., Rosenfield, J., & Fleming, E. (2001). An interactive model study of the influence of the Mount Pinatubo aerosol on stratospheric methane and water trends. *Journal of Geophysical Research*, 106(D21), 27711–27727. <https://doi.org/10.1029/2001JD000331>
- DallaSanta, K., Gerber, E. P., & Toohey, M. (2019). The circulation response to volcanic eruptions: The key roles of stratospheric warming and eddy interactions. *Journal of Climate*, 32(4), 1101–1120. <https://doi.org/10.1175/JCLI-D-18-0099.1>
- DallaSanta, K., Orbe, C., Rind, D., Nazarenko, L., & Jonas, J. (2021). Response of the Quasi-Biennial Oscillation to historical volcanic eruptions. *Geophysical Research Letters*, 48(20), e2021GL095412. <https://doi.org/10.1029/2021GL095412>
- Dhomse, S., Emmerson, K. M., Mann, G. W., Bellouin, N., Carslaw, K. S., Chipperfield, M. P., et al. (2014). Aerosol microphysics simulations of the Mt. Pinatubo eruption with the UM-UKCA composition-climate model. *Atmospheric Chemistry and Physics*, 14(20), 11221–11246. <https://doi.org/10.5194/acp-14-11221-2014>
- Dhomse, S., Weber, M., & Burrows, J. (2008). The relationship between tropospheric wave forcing and tropical lower stratospheric water vapor. *Atmospheric Chemistry and Physics*, 8(3), 471–480. <https://doi.org/10.5194/acp-8-471-2008>
- Diallo, M., Legras, B., & Chédin, A. (2012). Age of stratospheric air in the ERA-Interim. *Atmospheric Chemistry and Physics*, 12(24), 12133–12154. <https://doi.org/10.5194/acp-12-12133-2012>
- Diallo, M., Ploeger, F., Konopka, P., Birner, T., Müller, R., Riese, M., et al. (2017). Significant contributions of volcanic aerosols to decadal changes in the stratospheric circulation. *Geophysical Research Letters*, 44(20), 10780–10791. <https://doi.org/10.1002/2017GL074662>
- Dlugokencky, E. J., Dutton, E. G., Novelli, P. C., Tans, P. P., Masarie, K. A., Lantz, K. O., & Madronich, S. (1996). Changes in CH₄ and CO growth rates after the eruption of Mt. Pinatubo and their link with changes in tropical tropospheric UV flux. *Geophysical Research Letters*, 23(20), 2761–2764. <https://doi.org/10.1029/96GL02638>
- Dlugokencky, E. J., Masarie, K. A., Lang, P. M., Tans, P. P., Steele, L. P., & Nisbet, E. G. (1994). A dramatic decrease in the growth rate of atmospheric methane in the northern hemisphere during 1992. *Geophysical Research Letters*, 21(1), 45–48. <https://doi.org/10.1029/93GL03070>
- Domeisen, D. I. V., Garfinkel, C. I., & Butler, A. H. (2019). The teleconnection of El Niño Southern Oscillation to the stratosphere. *Reviews of Geophysics*, 57(1), 5–47. <https://doi.org/10.1029/2018RG000596>
- Eichinger, R., Dietmüller, S., Garny, H., Šácha, P., Birner, T., Bönišch, H., et al. (2019). The influence of mixing on the stratospheric age of air changes in the 21st century. *Atmospheric Chemistry and Physics*, 19(2), 921–940. <https://doi.org/10.5194/acp-19-921-2019>
- Evans, S. J., Toumi, R., Harries, J. E., Chipperfield, M. R., & Russell, J. M., III. (1998). Trends in stratospheric humidity and the sensitivity of ozone to these trends. *Journal of Geophysical Research*, 103(D8), 8715–8725. <https://doi.org/10.1029/98JD00265>
- Fueglistaler, S. (2012). Stepwise changes in stratospheric water vapor? *Journal of Geophysical Research*, 117(D13), D13302. <https://doi.org/10.1029/2012JD017582>
- Garcia, R. R., Randel, W. J., & Kinnison, D. E. (2011). On the determination of age of air trends from atmospheric trace species. *Journal of the Atmospheric Sciences*, 68(1), 139–154. <https://doi.org/10.1175/2010JAS3527.1>
- Garfinkel, C. I., Aquila, V., Waugh, D. W., & Oman, L. D. (2017). Time-varying changes in the simulated structure of the Brewer–Dobson circulation. *Atmospheric Chemistry and Physics*, 17(2), 1313–1327. <https://doi.org/10.5194/acp-17-1313-2017>
- Garfinkel, C. I., Gordon, A., Oman, L. D., Li, F., Davis, S., & Pawson, S. (2018). Nonlinear response of tropical lower-stratospheric temperature and water vapor to ENSO. *Atmospheric Chemistry and Physics*, 18(7), 4597–4615. <https://doi.org/10.5194/acp-18-4597-2018>
- Garfinkel, C. I., Harari, O., Ziskin Ziv, S., Rao, J., Morgenstern, O., Zeng, G., et al. (2021). Influence of the El Niño–Southern Oscillation on entry stratospheric water vapor in coupled chemistry–ocean CCM1 and CMIP6 models. *Atmospheric Chemistry and Physics*, 21(5), 3725–3740. <https://doi.org/10.5194/acp-21-3725-2021>
- Garfinkel, C. I., Waugh, D. W., Oman, L. D., Wang, L., & Hurwitz, M. M. (2013). Temperature trends in the tropical upper troposphere and lower stratosphere: Connections with sea surface temperatures and implications for water vapor and ozone. *Journal of Geophysical Research*, 118(17), 9658–9672. <https://doi.org/10.1002/jgrd.50772>
- Harris, C. R., Millman, K. J., van der Walt, S. J., Gommers, R., Virtanen, P., Cournapeau, D., et al. (2020). Array programming with NumPy. *Nature*, 585(7825), 357–362. <https://doi.org/10.1038/s41586-020-2649-2>
- Hofmann, D. J., & Solomon, S. (1989). Ozone destruction through heterogeneous chemistry following the eruption of El Chichón. *Journal of Geophysical Research*, 94(D4), 5029–5041. <https://doi.org/10.1029/JD094iD04p05029>
- Holton, J. R., Haynes, P. H., McIntyre, M. E., Douglass, A. R., Rood, R. B., & Pfister, L. (1995). Stratosphere–troposphere exchange. *Reviews of Geophysics*, 33(4), 403–439. <https://doi.org/10.1029/95RG02097>
- Hoyer, S., Fitzgerald, C., Hamman, J., Akleeman, A., Kluyver, T., Roos, M., et al. (2022). xarray (v2022.06.0). *Zenodo*. <https://doi.org/10.5281/zenodo.6885151>
- Hunter, J. D. (2007). Matplotlib: A 2D graphics environment. *Computing in Science & Engineering*, 9(03), 90–95. <https://doi.org/10.1109/mcse.2007.55>
- Joshi, M. M., & Jones, G. S. (2009). The climatic effects of the direct injection of water vapour into the stratosphere by large volcanic eruptions. *Atmospheric Chemistry and Physics*, 9(16), 6109–6118. <https://doi.org/10.5194/acp-9-6109-2009>
- Joshi, M. M., & Shine, K. P. (2003). A GCM study of volcanic eruptions as a cause of increased stratospheric water vapor. *Journal of Climate*, 16(21), 3525–3534. [https://doi.org/10.1175/1520-0442\(2003\)016<3525:AGSOVE>2.0.CO;2](https://doi.org/10.1175/1520-0442(2003)016<3525:AGSOVE>2.0.CO;2)
- Jucker, M. (2022). mjucker/aostools: Aostools v2.4. *Zenodo*. <https://doi.org/10.5281/zenodo.6486829>

- Kilian, M., Brinkop, S., & Jöckel, P. (2020). Impact of the eruption of Mt Pinatubo on the chemical composition of the stratosphere. *Atmospheric Chemistry and Physics*, 20(20), 11697–11715. <https://doi.org/10.5194/acp-20-11697-2020>
- Kinne, S., Toon, O. B., & Prather, M. J. (1992). Buffering of stratospheric circulation by changing amounts of tropical ozone: A Pinatubo case study. *Geophysical Research Letters*, 19, 1927–1930. <https://doi.org/10.1029/92GL01937>
- Kroll, C. A., Dacie, S., Azoulay, A., Schmidt, H., & Timmreck, C. (2021). The impact of volcanic eruptions of different magnitude on stratospheric water vapor in the tropics. *Atmospheric Chemistry and Physics*, 21(8), 6565–6591. <https://doi.org/10.5194/acp-21-6565-2021>
- Lacis, A., Hansen, J., & Sato, M. (1992). Climate forcing by stratospheric aerosols. *Geophysical Research Letters*, 19(15), 1607–1610. <https://doi.org/10.1029/92GL01620>
- Löffler, M., Brinkop, S., & Jöckel, P. (2016). Impact of major volcanic eruptions on stratospheric water vapour. *Atmospheric Chemistry and Physics*, 16(10), 6547–6562. <https://doi.org/10.5194/acp-16-6547-2016>
- Mann, G. W., Carslaw, K. S., Spracklen, D. V., Ridley, D. A., Manktelow, P. T., Chipperfield, M. P., et al. (2010). Description and evaluation of GLOMAP-mode: A modal global aerosol microphysics model for the UKCA composition-climate model. *Geoscientific Model Development*, 3(2), 519–551. <https://doi.org/10.5194/gmd-3-519-2010>
- Millán, L., Santee, M. L., Lambert, A., Livesey, N. J., Werner, F., Schwartz, M. J., et al. (2022). The Hunga Tonga-Hunga Ha'apai hydration of the stratosphere. *Geophysical Research Letters*, 49(13), e2022GL099381. <https://doi.org/10.1029/2022GL099381>
- Ming, A., & Hitchcock, P. (2022). What contributes to the inter-annual variability in tropical lower stratospheric temperatures? *Journal of Geophysical Research*, 127(1), e2021JD035548. <https://doi.org/10.1029/2021JD035548>
- Mote, P. W., Rosenlof, K. H., McIntyre, M. E., Carr, E. S., Gille, J. C., Holton, J. R., et al. (1996). An atmospheric tape recorder: The imprint of tropical tropopause temperatures on stratospheric water vapor. *Journal of Geophysical Research*, 101(D2), 3989–4006. <https://doi.org/10.1029/95JD03422>
- Mulcahy, J. P., Jones, C., Sellar, A., Johnson, B., Boutle, I. A., Jones, A., et al. (2018). Improved aerosol processes and effective radiative forcing in HadGEM3 and UKESM1. *Journal of Advances in Modeling Earth Systems*, 10(11), 2786–2805. <https://doi.org/10.1029/2018MS001464>
- Muthers, S., Kuchar, A., Stenke, A., Schmitt, J., Anet, J. G., Raible, C. C., & Stocker, T. F. (2016). Stratospheric age of air variations between 1600 and 2100. *Geophysical Research Letters*, 43(10), 5409–5418. <https://doi.org/10.1002/2016GL068734>
- Pitari, G. (1993). A numerical study of the possible perturbation of stratospheric dynamics due to Pinatubo aerosols: Implications for tracer transport. *Journal of the Atmospheric Sciences*, 50(15), 2443–2461. [https://doi.org/10.1175/1520-0469\(1993\)050<2443:ANSOTP>2.0.CO;2](https://doi.org/10.1175/1520-0469(1993)050<2443:ANSOTP>2.0.CO;2)
- Pitari, G., & Mancini, E. (2002). Short-term climatic impact of the 1991 volcanic eruption of Mt. Pinatubo and effects on atmospheric tracers. *Natural Hazards and Earth System Sciences*, 2(1/2), 91–108. <https://doi.org/10.5194/nhess-2-91-2002>
- Randel, W. J., Garcia, R., & Wu, F. (2008). Dynamical balances and tropical stratospheric upwelling. *Journal of the Atmospheric Sciences*, 65(11), 3584–3595. <https://doi.org/10.1175/2008JAS2756.1>
- Randel, W. J., Wu, F., Vömel, H., Nedoluha, G. E., & Forster, P. (2006). Decreases in stratospheric water vapor after 2001: Links to changes in the tropical tropopause and the Brewer-Dobson circulation. *Journal of Geophysical Research*, 111(D12), D12312. <https://doi.org/10.1029/2005JD006744>
- Richter, J. H., Tilmes, S., Mills, M. J., Tribbia, J. J., Kravitz, B., MacMartin, D. G., et al. (2017). Stratospheric dynamical response and ozone feedbacks in the presence of SO₂ injections. *Journal of Geophysical Research*, 122(23), 12557–12573. <https://doi.org/10.1002/2017JD026912>
- Rieger, L. A., Cole, J. N. S., Fyfe, J. C., Po-Chedley, S., Cameron-Smith, P. J., Durack, P. J., et al. (2020). Quantifying CanESM5 and EAMv1 sensitivities to Mt. Pinatubo volcanic forcing for the CMIP6 historical experiment. *Geosci. Model Dev*, 13(10), 4831–4843. <https://doi.org/10.5194/gmd-13-4831-2020>
- Robock, A. (2000). Volcanic eruptions and climate. *Reviews of Geophysics*, 38(2), 191–219. <https://doi.org/10.1029/1998RG000054>
- Rosenlof, K. H., Oltmans, S., Kley, D., Russell, J., Chiou, E. W., Chu, W., et al. (2001). Stratospheric water vapor increases over the past half-century. *Geophysical Research Letters*, 28(7), 1195–1198. <https://doi.org/10.1029/2000GL012502>
- Rosenlof, K. H., & Reid, G. C. (2008). Trends in the temperature and water vapor content of the tropical lower stratosphere: Sea surface connection. *Journal of Geophysical Research*, 113(D6), D06107. <https://doi.org/10.1029/2007jd009109>
- Scaife, A. A., Butchart, N., Jackson, D. R., & Swinbank, R. (2003). Can changes in ENSO activity help to explain increasing stratospheric water vapor? *Geophysical Research Letters*, 30(17). <https://doi.org/10.1029/2003GL017591>
- Self, S. (1992). Krakatau revisited: The course of events and interpretation of the 1883 eruption. *Geojournal*, 28(2), 109–121. <https://doi.org/10.1007/BF00177223>
- Self, S., & Sparks, R. S. J. (1978). Characteristics of widespread pyroclastic deposits formed by the interaction of silicic magma and water. *Bulletin Volcanologique*, 41(3), 196–212. <https://doi.org/10.1007/BF02597223>
- Sellar, A. A., Jones, C. G., Mulcahy, J. P., Tang, Y., Yool, A., Wiltshire, A., et al. (2019). UKESM1: Description and evaluation of the UK Earth system model. *Journal of Advances in Modeling Earth Systems*, 11(12), 4513–4558. <https://doi.org/10.1029/2019MS001739>
- Seviour, W. J. M., Butchart, N., & Hardiman, S. C. (2012). The Brewer–Dobson circulation inferred from ERA-Interim. *Quarterly Journal of the Royal Meteorological Society*, 138(665), 878–888. <https://doi.org/10.1002/qj.966>
- Stenchikov, G., Ukhov, A., Osipov, S., Ahmadov, R., Grell, G., Cady-Pereira, K., et al. (2021). How does a Pinatubo-size volcanic cloud reach the middle stratosphere? *Journal of Geophysical Research*, 126(10), e2020JD033829. <https://doi.org/10.1029/2020JD033829>
- Stenchikov, G. L., Kirchner, I., Robock, A., Graf, H.-F., Antuña, J. C., Grainger, R. G., et al. (1998). Radiative forcing from the 1991 Mount Pinatubo volcanic eruption. *Journal of Geophysical Research*, 103(D12), 13837–13857. <https://doi.org/10.1029/98JD00693>
- Storkey, D., Blaker, A. T., Mathiot, P., Megann, A., Akseonov, Y., Blockley, E. W., et al. (2018). UK global ocean G06 and G07: A traceable hierarchy of model resolutions. *Geoscientific Model Development*, 11(8), 3187–3213. <https://doi.org/10.5194/gmd-11-3187-2018>
- Thompson, D. W., & Solomon, S. (2005). Recent stratospheric climate trends as evidenced in radiosonde data: Global structure and tropospheric linkages. *Journal of Climate*, 18(22), 4785–4795. <https://doi.org/10.1175/JCLI3585.1>
- Toohey, M., Krüger, K., Bittner, M., Timmreck, C., & Schmidt, H. (2014). The impact of volcanic aerosol on the Northern Hemisphere stratospheric polar vortex: Mechanisms and sensitivity to forcing structure. *Atmospheric Chemistry and Physics*, 14(23), 13063–13079. <https://doi.org/10.5194/acp-14-13063-2014>
- Virtanen, P., Gommers, R., Oliphant, T. E., Haberland, M., Reddy, T., Cournapeau, D., et al. (2020). SciPy 1.0: Fundamental algorithms for scientific computing in Python. *Nature Methods*, 17(3), 261–272. <https://doi.org/10.1038/s41592-019-0686-2>
- Walters, D., Baran, A. J., Boutle, I., Brooks, M., Earnshaw, P., Edwards, J., et al. (2019). The Met Office unified model global atmosphere 7.0/7.1 and JULES global land 7.0 configurations. *Geoscientific Model Development*, 12(5), 1909–1963. <https://doi.org/10.5194/gmd-12-1909-2019>
- Zanchettin, D., Khodri, M., Timmreck, C., Toohey, M., Schmidt, A., Gerber, E. P., et al. (2016). The model intercomparison project on the climatic response to volcanic forcing (VolMIP): Experimental design and forcing input data for CMIP6. *Geoscientific Model Development*, 9(8), 2701–2719. <https://doi.org/10.5194/gmd-9-2701-2016>

- Zanchettin, D., Timmreck, C., Khodri, M., Cole, J. N. S., Tsigaridis, K., Abe, M., & Mann, G. (2022b). VolMIP piControl field-average GL TR NH SH ENSO NAO monthly time series. In *World data center for climate (WDCC) at DKRZ*. https://doi.org/10.26050/WDCC/VolMIP_pC
- Zanchettin, D., Timmreck, C., Khodri, M., Cole, J. N. S., Tsigaridis, K., Abe, M., & Mann, G. (2022c). VolMIP volc-pinatubo-full field-average GL TR NH SH ENSO NAO monthly time series. In *World data center for climate (WDCC) at DKRZ*. https://doi.org/10.26050/WDCC/VolMIP_volc
- Zanchettin, D., Timmreck, C., Khodri, M., Schmidt, A., Toohy, M., Abe, M., et al. (2022a). Effects of forcing differences and initial conditions on inter-model agreement in the VolMIP volc-pinatubo-full experiment. *Geoscientific Model Development*, 15(5), 2265–2292. <https://doi.org/10.5194/gmd-15-2265-2022>
- Zhou (2023). XinZhou-1/GRL-Data-Archive: Version1 (v1.0.0). *Zenodo*. <https://doi.org/10.5281/zenodo.7810072>